
CMB Anisotropies: A Decadal Survey

Wayne Hu

Institute for Advanced Study, Princeton, NJ, 08540, USA, whu@ias.edu

Said the disciple, “After I heard your words, one year and I ran wild, two years and I was tame, three years and positions interchanged, four years and things settled down, five years and things came to me, nine years and I had the great secret.”

–Chuang-tzu

Abstract

We review the theoretical implications of the past decade of CMB anisotropy measurements, which culminated in the recent detection of the first feature in the power spectrum, and discuss the tests available to the next decade of experiments. The current data already suggest that density perturbations originated in an inflationary epoch, the universe is spatially flat, and baryonic dark matter is required. We discuss the underlying assumptions of these claims and outline the tests required to ensure they are robust. The most critical test - the presence of a second feature at the predicted location - should soon be available. Further in the future, secondary anisotropies and polarization should open new windows to the early and low(er) redshift universe.

1 Introduction

The 1990’s will be remembered as a decade of discovery for cosmic microwave background (CMB) anisotropies. The launch of the COBE satellite ushered in the decade in 1990 and led to the first detection of CMB anisotropies at $> 10^\circ$ scales [1]. Through the decade, a combination of higher resolution experiments made the case for a rise in the anisotropy level on degree scales and a subsequent fall at arcminute scales [2]. The final year saw experiments, notably Toco and Boomerang, with sufficient angular resolution and sky coverage to localize a sharp peak in the anisotropy spectrum at approximately 0.5° [3]. In this review, we discuss the theoretical implications of these results and provide a roadmap for critical tests and uses of CMB anisotropies in the coming decade.

2 Once and Future Power Spectrum

The tiny 10^{-5} variations in the temperature of the CMB across the sky are observed to be consistent with Gaussian random fluctuations, at least on the COBE scales ($> 10^\circ$), as expected in the simplest theories of their inflationary origin. Assuming Gaussianity, the fluctuations can be fully characterized by their angular power spectrum¹

$$T(\hat{\mathbf{n}}) = \sum_{\ell m} a_{\ell m} Y_{\ell m}(\hat{\mathbf{n}}), \quad \langle a_{\ell m}^* a_{\ell' m'} \rangle = \delta_{\ell\ell'} \delta_{mm'} C_\ell. \quad (1)$$

We will often use the shorthand $(\Delta T)^2 = \ell(\ell + 1)C_\ell/2\pi$ which represents the power per logarithmic interval in ℓ .

¹ Conventions for relating multipole number to angular scale include: $\theta_\ell \approx 2\pi/\ell$, π/ℓ or $100^\circ/\ell$. To the extent that these conventions differ, none of them are correct; we hereafter refer to power spectrum features by multipole number, which has a precise meaning.

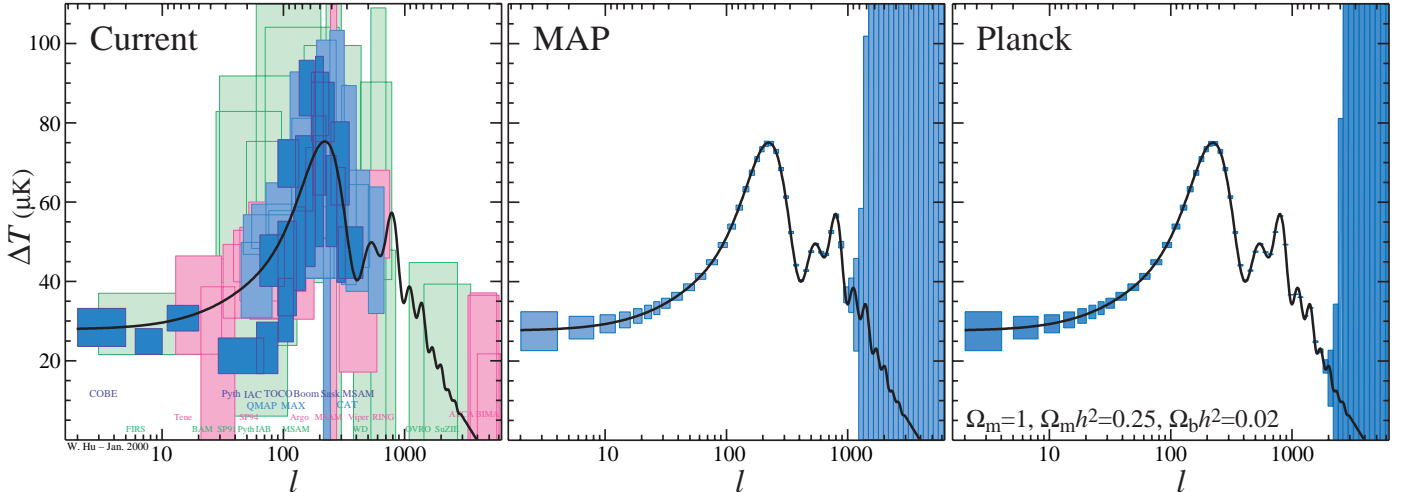


Fig. 1: Power Spectrum

Fig. 1 (left, 1σ errors \times window FWHM) shows the measurements the power spectrum to date (see [3] for a complete list of references). The data indicate a rather sharp peak in the spectrum at $\ell \sim 200$ with a significant decline at $\ell \gtrsim 1000$. This peak has profound implications for cosmology. The primary claims in decreasing order of confidence and increasing need of verification from precision measurements (e.g. from the MAP and Planck satellite Fig. 1 center, right) are

- Early universe. The simplest inflationary cold dark matter (CDM) cosmologies have correctly predicted the location and morphology of the first peak in the CMB; conversely, all competing *ab initio* theories have failed, essentially due to causality. *Confirm its acoustic nature with the second peak. Use polarization as a sharp test of causality.*
- Geometry. The universe is flat. *Lower limits on the total density ($\Omega_{tot} \equiv \sum \Omega_i \gtrsim 0.6$ [3]) are already robust, unless recombination is substantially delayed or $h \gg 1$. Calibrate the “standard rulers” (acoustic scale and damping scale) in this distance measure through the higher peaks.*
- Baryons. At least as much baryonic dark matter as indicated by big bang nucleosynthesis (BBN) is required ($\Omega_b h^2 \gtrsim 0.01$ [3]). *Confirm with relative heights of the peaks, especially the third peak.*
- Reionization. The Thomson optical depth is low – how low depends on the range of models considered. *The optical depth, assuming it is low, will only be accurately measured by CMB polarization at large angles.*
- Dark energy. The matter density is low and combined with flatness, this indicates a missing energy component, possibly the cosmological constant. Currently the 95% CL includes $\Omega_m = 1$ but the maximum likelihood model including BBN and h constraints has $\Omega_m \approx 0.3$ [3]. *Measure $\Omega_m h^2$ from the first three peaks.*

The early universe and geometry tests basically rely on the position of the first peak and hence are more robust than the later ones which rely mainly on interpreting its amplitude.

Moreover, all claims are based on interpreting the peak at $\ell \sim 200$ as the first in a series of *acoustic peaks*. Based on the sharpness of the feature, this interpretation is now reasonably, but not completely secure. The detection of a second peak in the spectrum is critical since it will provide essentially incontrovertible evidence that this interpretation is correct (or wrong!). Once this is achieved and the peaks pass the morphological tests described below, the CMB will become the premier laboratory for precision cosmology, as many studies have shown [4]. These expectations also rely on the fact that C_ℓ can ultimately be measured to

$$\frac{\Delta C_\ell}{C_\ell} = \sqrt{\frac{2}{(2\ell + 1)f_{\text{sky}}}}, \quad (2)$$

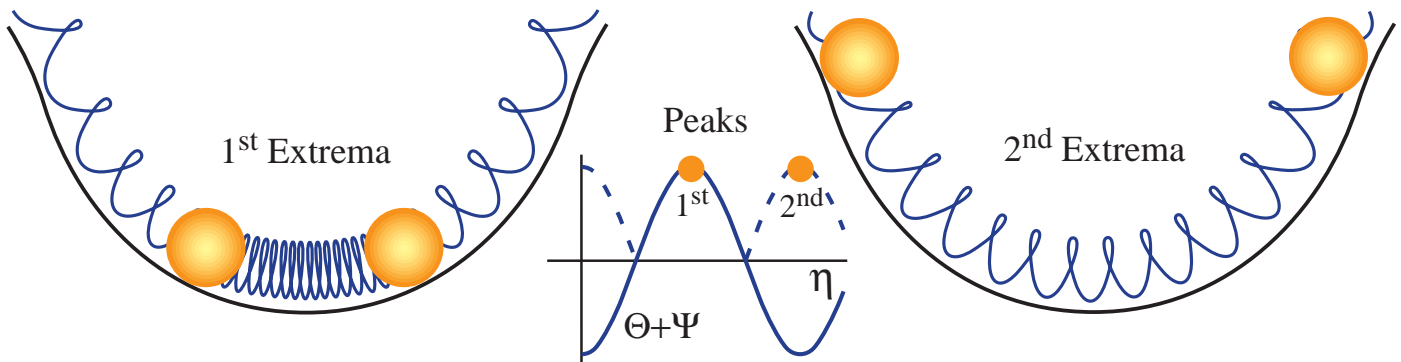


Fig. 2: Harmonic Acoustic Peaks.

based on Gaussian sample variance on the $(2\ell + 1)f_{\text{sky}}$ independent modes of a given ℓ , from a fraction of sky f_{sky} . The rest of this review will make the theoretical case for the above statements.

3 Sound Physics

The theory underlying the predictions of CMB anisotropies has essentially been in place since the 1970's [5] and is based on extraordinarily simple fluid mechanics and gravity [6, 7]. Simplicity is ensured by the smallness of the fluctuations themselves: the observed amplitude of $\Delta T/T \sim 10^{-5}$ guarantees that the equations of motion can be linearized.

The fluid nature of the problem follows from simple thermal arguments. The cooling of CMB photons due to the cosmological expansion implies that before $z_* \approx 1000$, when the CMB temperature is $T > 3000\text{K}$, the photons are hot enough to ionize hydrogen. During this epoch, the electrons glue the baryons to the photons by Compton scattering and electromagnetic interactions. The dynamics that result involve a single photon-baryon fluid.

Gravity attracts and compresses the fluid into the potential wells that later seed large-scale structure. Photon pressure resists this compression and sets up sound waves or acoustic oscillations in the fluid. These sound waves are frozen into the CMB at recombination. Regions that have reached their maximal compression by recombination become hot spots on the sky; those that reach maximum rarefaction become cold spots.

4 Math

Mathematically, the cast of characters are: for the photons, the local temperature $\Theta = \Delta T/T$, bulk velocity or dipole v_γ , and anisotropic stress or quadrupole π_γ ; for the baryons, the density perturbation δ_b and bulk velocity v_b ; for gravity, the Newtonian potential Ψ (time-time metric fluctuation) and the curvature fluctuation Φ (space-space metric fluctuation $\approx -\Psi$). Covariant conservation of energy and momentum requires that the photons and baryons satisfy separate continuity equations [6]

$$\dot{\Theta} = -\frac{k}{3}v_\gamma - \dot{\Phi}, \quad \dot{\delta}_b = -kv_b - 3\dot{\Phi}, \quad (3)$$

and Euler equations

$$\dot{v}_\gamma = k(\Theta + \Psi) - \frac{k}{6}[1 + 3(1 - \Omega_{\text{tot}})\frac{H_0^2}{k^2}]\pi_\gamma - \dot{\tau}(v_\gamma - v_b),$$

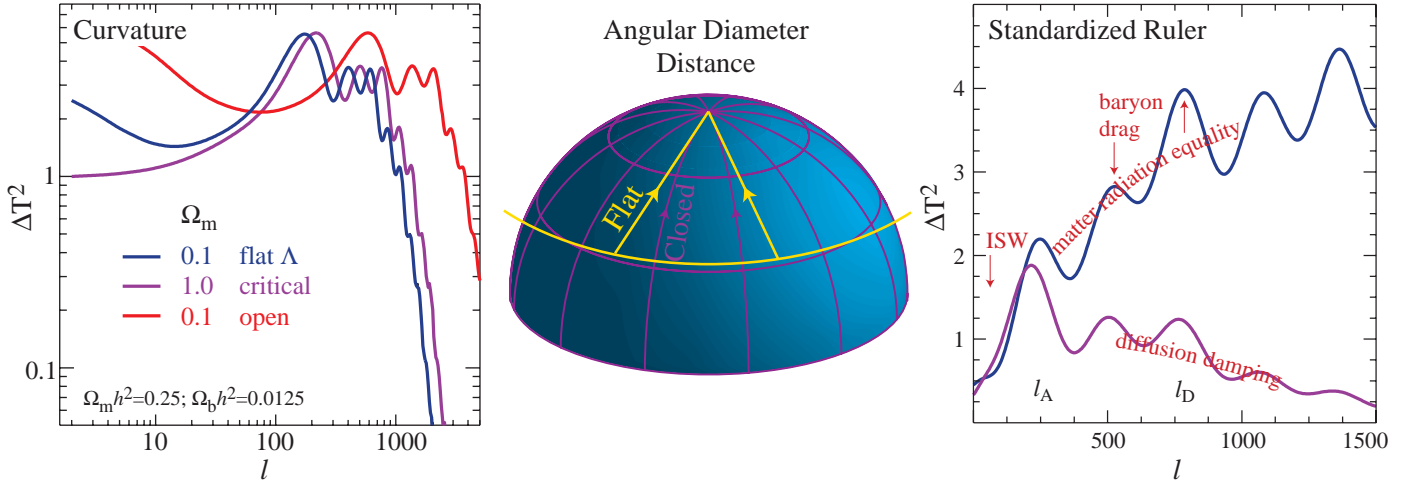


Fig. 3: Geometry.

$$\dot{v}_b = -\frac{\dot{a}}{a}v_b + k\Psi + \dot{\tau}(v_\gamma - v_b)/R, \quad (4)$$

in wavenumber space. $\dot{\tau} = n_e\sigma_T a$ is the differential Thomson optical depth, $R = (p_b + \rho_b)/(p_\gamma + \rho_\gamma) \approx 3\rho_b/4\rho_\gamma$ is the photon-baryon momentum density ratio, and overdots represent derivatives with respect to conformal time $\eta = \int dt/a$.

The continuity equations represent particle number conservation. For the baryons, $\rho_b \propto n_b$. For the photons, $T \propto n_\gamma^{1/3}$, which explains the $1/3$ in the velocity divergence term. The $\dot{\Phi}$ term represents the “metric stretching” effect and appears because Φ represents a spatially varying perturbation to the scale factor a and $n_{\gamma,b} \propto a^{-3}$ (see Fig. 7, left).

The Euler equation has a similar interpretation. The expansion makes particle momenta decay as a^{-1} . The cosmological redshift of T accounts for this effect in the photons. For the baryons, it becomes the expansion drag on v_b (\dot{a}/a term). Potential gradients $k\Psi$ generate potential flow. For the photons, stress gradients in the fluid, both isotropic ($k\delta p_\gamma/(p_\gamma + \rho_\gamma) = k\Theta$) and anisotropic ($k\pi_\gamma$) counter infall. Compton scattering exchanges momentum between the two fluids ($\dot{\tau}$ terms).

If scattering ($\dot{\tau}^{-1}$) is rapid compared with the light travel time across the perturbation (k^{-1}), the photon-baryon system behaves as a perfect fluid. To lowest order in $k/\dot{\tau}$, eqns. (3) and (4) become

$$(m_{\text{eff}}\dot{\Theta}) + \frac{k^2}{3}\Theta = -\frac{k^2}{3}m_{\text{eff}}\Psi - (m_{\text{eff}}\dot{\Phi}), \quad (5)$$

where the effective mass is $m_{\text{eff}} = 1 + R$ or alternatively $c_s^2 = \dot{p}/\dot{\rho} = 1/3m_{\text{eff}}$. Scattering isotropizes the distribution in the electron rest frame $v_\gamma = v_b$ and eliminates anisotropic stress ($\pi_\gamma = \mathcal{O}(k/\dot{\tau})v_\gamma$).

Equation (5) is the fundamental relation for acoustic oscillations; it reads: the change in the momentum of the photon-baryon fluid is determined by a competition between the pressure restoring and gravitational driving forces. Given the initial conditions and gravitational potentials, it predicts the phenomenology of the acoustic peaks.

5 Early Universe

The simplest inflationary models are essentially unique in their phenomenological predictions. They possess a spectrum of curvature (potential) fluctuations that extends *outside* the apparent horizon in

the post-inflationary epoch. These perturbations remain constant while the fluctuation is outside the horizon except for a small change at matter-radiation equality. Neglecting this and baryon inertia ($m_{\text{eff}} = 1$) for the moment, the oscillator equation (5) has the simple solution

$$[\Theta + \Psi](\eta_*) = [\Theta + \Psi](0) \cos(ks), \quad v_\gamma = \sqrt{3}[\Theta + \Psi](0) \sin(ks), \quad (6)$$

where $s = \int_0^{\eta_*} c_s d\eta$ is the *sound horizon* at η_* . An initial temperature perturbation $\Theta(0)$ exists since the gravitational potential Ψ is a time-time perturbation to the metric. Because of the redshift with the scale factor $a \propto t^{2/3(1+p/\rho)}$, a temporal shift produces a temperature perturbation of $\Theta = -2\Psi/3(1+p/\rho)$ or $-\Psi/2$ in the radiation dominated era. We call $\Theta + \Psi$ the effective temperature since it also accounts for the redshift a photon experiences when climbing out of a potential well [8]. The matter radiation transition simply makes $\Theta + \Psi = \Psi/3$.

There are two important aspects of this result. First, inflation sets the *temporal* phase of all wave-modes by starting them all at the initial epoch. Wavenumbers which hit their extrema at recombination are given by $k_m = m\pi/s$ and these mark the peaks of coherent oscillation in the power spectrum. Second, the first peak at $k = \pi/s$ represents a compression of the fluid in the gravitational potential well ($\Psi < 0$, see Fig. 2).

Without inflation to push perturbations superluminally outside the horizon, they must be generated by the causal motion of matter. One might think any anisotropies above the horizon scale at recombination projected on the sky (e.g. COBE) implies inflation. However these could instead be generated after recombination through gravitational redshifts (§9). To test inflation, one needs to isolate a particular epoch in time. The acoustic peaks provide one such opportunity; we shall see later that polarization provides another.

If the fluctuations were generated by non-linear dynamics well inside the horizon, e.g. by a cosmic string network, the temporal coherence, and hence the peak structures, would be lost due to random forcing of the oscillators [9]. Causal generation itself does not guarantee incoherence. Coherence requires that there is one special epoch for all modes that synchs up their oscillations. One common event can causally achieve this: horizon crossing when $k\eta = 1$. For example, textures unwind at horizon crossing and maintain some coherence in their acoustic oscillations. However it is very difficult to place the first compressional peak at as large a scale as $k_1 = \pi/s$ since the photons tend to first cool down due to metric stretching from Φ as gravitational potentials grow, thus inhibiting the compressional heating [10]. The only known mechanism for doing so is to reverse the sign of gravity: to make gravitational potential wells in underdense regions so that $\Phi \sim \Psi$ [11]. In principle, this can be arranged by a special choice of anisotropic stresses but there is no known form of matter that obeys the required relations. On the other hand, *inflationary* curvature (adiabatic) and isocurvature (stress) fluctuations existing outside the horizon can be interconverted with physically realizable stress histories [12].

In summary, verification of an inflationary series of acoustic peaks with locations in an approximate ratio of $\ell_1 : \ell_2 : \ell_3 \dots = 1 : 2 : 3 \dots$ would represent a strong test of the inflationary origin of the perturbations and a somewhat weaker test of their initially adiabatic nature.

6 Geometry

The physical scale of the features is related to the distance s that sound can travel by recombination. Specifically, one expects features in the spatial power spectrum of the photon temperature and dipole at $k > k_A = \pi/s$. Each mode is then projected on the sky in spherical coordinates $\exp(i\mathbf{k} \cdot \mathbf{x}) \propto j_\ell(kd)Y_{\ell 0}$,

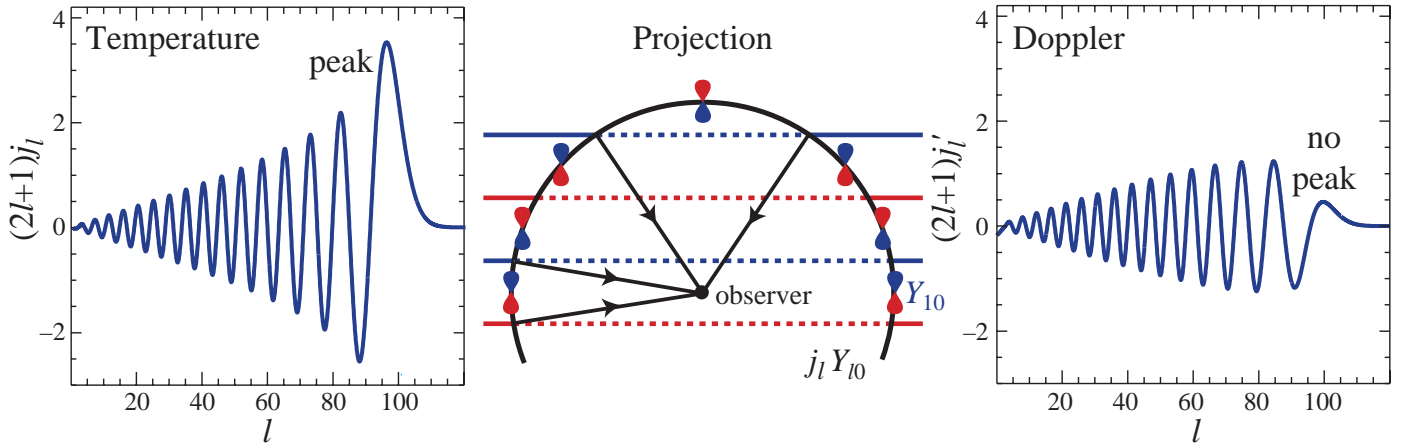


Fig. 4: Acoustic not Doppler peaks.

where $d = \eta_0 - \eta_*$, and summed in quadrature to form the final anisotropy,

$$C_\ell \approx \frac{2}{\pi} \int \frac{dk}{k} k^3 [(\Theta + \Psi)j_\ell(kd) + v_\gamma j'_\ell(kd)]^2. \quad (7)$$

This approximation ignores the finite duration of recombination but suffices for a qualitative understanding of the spectrum. We have also temporarily assumed that the universe is flat $\Omega_{\text{tot}} = 1$.

The v_γ term represents the Doppler effect from the motion of the fluid along the line of sight. It has an intrinsic dipole angular dependence at last scattering Y_{l0} in addition to the “orbital” angular dependence $Y_{\ell 0}$. Addition of angular momentum implies a coupling of $j_{\ell \pm 1}$ that can be rewritten as j'_ℓ .

As a consequence of eqn. (7), features in the spatial power spectrum of the effective temperature at recombination become features in the angular power spectrum whereas those of the bulk velocity do not (see Fig. 4 $kd = 100$) [6]. A plane wave temperature perturbation contributes a range of anisotropies corresponds to viewing angles perpendicular ($\ell \approx kd$) all the way to parallel ($\ell \rightarrow 0$) to the wavevector \mathbf{k} (see Fig. 4, lobes). The result is a sharp maximum around $\ell = kd$ as expected from naively converting physical to angular scale. However for the Doppler effect from potential flows, velocities are directed parallel to \mathbf{k} , so that the peak at $\ell = kd$ is eliminated. Although the Doppler effect contributes significantly to the overall anisotropy, the peak structure traces the temperature fluctuations.

In a spatially curved universe, one replaces the spherical Bessel functions in eqn. (7) with the ultraspherical Bessel functions and these peak at $\ell \approx kD$ where D is the *comoving angular diameter distance* to recombination. Consider first a closed universe with radius of curvature $\mathcal{R} = H_0 |\Omega_{\text{tot}} - 1|^{1/2}$. Suppressing one spatial coordinate yields a 2-sphere geometry with the observer situated at the pole (see Fig. 3). Light travels on lines of longitude. A physical scale λ at fixed latitude given by the polar angle θ subtends an angle $\alpha = \lambda/\mathcal{R} \sin \theta$. For $\alpha \ll 1$, a Euclidean analysis would infer a distance $D = \mathcal{R} \sin \theta$, even though the *coordinate distance* along the arc is $d = \theta \mathcal{R}$; thus

$$D = \mathcal{R} \sin(d/\mathcal{R}), \quad (\Omega_{\text{tot}} > 1). \quad (8)$$

For open universes, simply replace \sin with \sinh . A given physical scale subtends a larger (smaller) angle in a closed (open) universe than a flat universe.

We thus expect CMB features at the characteristic scale [13]

$$\ell_A = \pi D/s \approx 172 \Omega_{\text{tot}}^{-1/2} [1 + \ln(1 - \Omega_\Lambda)]^{0.085} f(\Omega_m h^2, \Omega_b h^2), \quad (9)$$

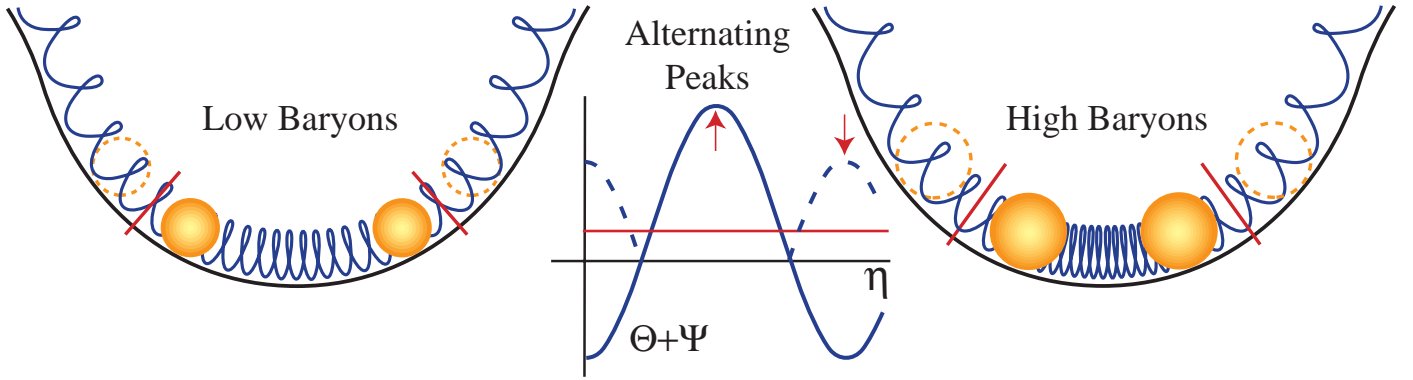


Fig. 5: Baryons.

$$f = \left(\frac{z_*}{10^3}\right)^{1/2} \left(\frac{1}{\sqrt{R_*}} \ln \frac{\sqrt{1+R_*} + \sqrt{R_* + \epsilon R_*}}{1 + \sqrt{\epsilon R_*}}\right)^{-1}, \quad (10)$$

where $\epsilon \equiv a_{eq}/a_* = 0.042(\Omega_m h^2)^{-1}(z_*/10^3)$ and $R_* = 30\Omega_b h^2(z_*/10^3)$; see [14] for $z_*(\Omega_m h^2, \Omega_b h^2)$.

The main scaling of ℓ_A is with $\Omega_{tot}^{-1/2}$ [15], but finite Ω_Λ causes it to decrease. This covariance is referred to in the literature as the *angular diameter distance (D) degeneracy*. The quantity in parentheses in eqn. (10) goes to unity as $\epsilon, R_* \rightarrow 0$. The leading order correction $(1 + \epsilon^{1/2})$ makes the $\Omega_m h^2$ dependence important in any reasonable cosmology. The other correction $(1 + R_*/6)$ is small for reasonable baryon densities.

For simple inflationary models, the peaks reside at $\ell_m \approx m\ell_A$. More generally, $\ell_1 \geq \ell_A$ (see §5). The detection of the first peak then puts a reasonably robust lower limit on Ω_{tot} . The key assumptions are that we can attribute the feature to acoustic oscillations, bound the redshift of recombination from below and bound the sound horizon from above. The last assumption amounts to having an upper limit on $\Omega_m h^2$ (or h). The D degeneracy is tamed since Ω_Λ is automatically bounded from above for the Ω_{tot} of interest by requiring $\Omega_m > 0$. Converting lower limits on Ω_{tot} into precise measurements requires independent measurements of $\Omega_m h^2$ and $\Omega_b h^2$, which calibrate the standard rulers at recombination [6], and Ω_Λ, Ω_m or h to break the D degeneracy.

7 Baryons

Baryons add inertia to the fluid. Consider first the case of $m_{eff} = 1 + R = \text{const.}$ [see eqn. (5)]

$$[\Theta + \Psi](\eta_*) = [\Theta(0) + (1 + R)\Psi(0)] \cos(ks) - R\Psi, \quad (11)$$

where $s = \eta_*/\sqrt{3(1+R)}$. There are three effects of raising the baryon content: an amplitude increase, a zero-point shift, and a frequency decrease [6]. Baryons drag the fluid deeper into the potential wells (see Fig. 5). For the fixed initial conditions, the resulting shift in the zero point also implies a larger amplitude. Since it is the power spectrum that is observed, the result of squaring implies that all compressional peaks are enhanced by the baryons and the rarefaction peaks suppressed. This is the clearest signature of the baryons and also provides a means for testing the compressional nature of the first peak predicted by inflation. The fact that $R \propto a$ due to the redshifting of the photons simply means that the oscillator actually has time dependent mass. The adiabatic invariant (E/ω) implies an amplitude reduction as $(1 + R)^{-1/4}$.

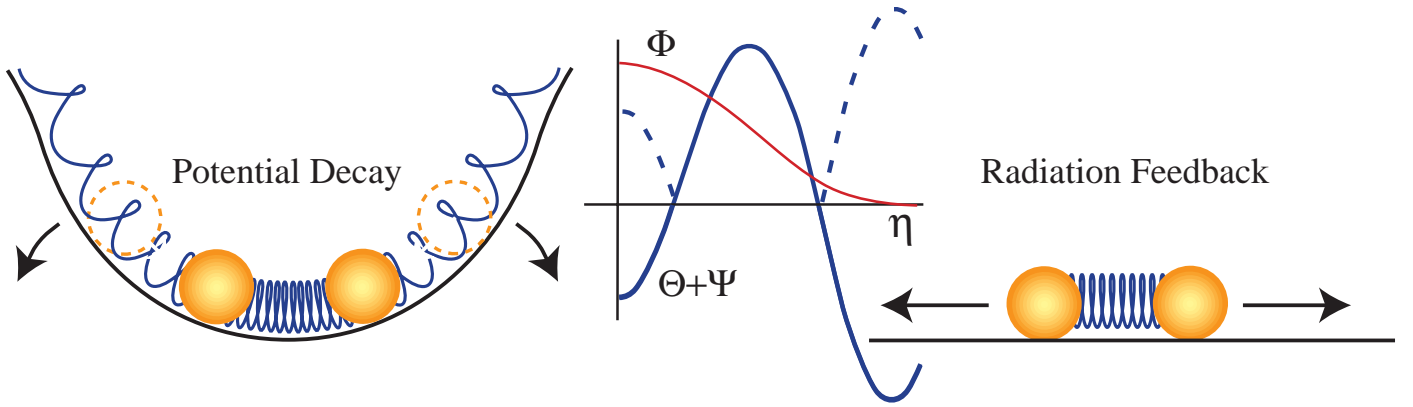


Fig. 6: Matter-radiation ratio.

Baryons also affect the fluid through dissipational processes [16]. The random walk of the photons through the baryons damps the acoustic oscillation exponentially below the diffusion scale k_D , roughly the geometric mean of the mean free path and the horizon scale. Microphysically, the dissipation comes from viscosity π_γ in eqn. (4) and heat conduction $v_\gamma - v_b$. Before recombination it can be included by keeping terms of order $k/\dot{\tau}$ in the equations. At recombination, the mean free path increases and brings the diffusion scale to [14]

$$k_D \approx a_1(\Omega_m h^2) (\Omega_b h^2)^{0.291} [1 + a_2(\Omega_m h^2) (\Omega_b h^2)^{1.8}]^{-1/5} \text{Mpc}^{-1}, \quad (12)$$

$a_1(x) = 0.0396x^{-0.248}(1 + 13.6x^{0.638})$, $a_2(x) = 1480x^{-0.0606}(1 + 10.2x^{0.553})^{-1}$. The main effects can be easily understood: increasing $\Omega_m h^2$ decreases the horizon at last scattering and hence the diffusion length. At low $\Omega_b h^2$, increasing the baryon content decreases the mean free path while at high $\Omega_b h^2$, it delays recombination and increases the diffusion length.

Damping introduces another length scale for the curvature test, $l_D = k_D D$; alternately $l_D/l_A = k_D/k_A = f(\Omega_m h^2, \Omega_b h^2)$ is independent of D and can measure this combination of parameters.

8 Matter/Radiation

We have hitherto been considering the gravitational force on the oscillators as constant in time. This can only be true for *growing* density fluctuations. The Poisson equation says that $\Phi \propto a^2 \rho \delta$, and the density redshifts with the expansion as $\rho \propto a^{-3(1+p/\rho)}$. In the radiation era, density perturbations must grow as a^2 for constant potentials, as they do in the comoving gauge when pressure gradients can be neglected. Once the pressure gradients have turned infall into acoustic oscillations, the potential must decay. This decay actually drives the oscillations since the fluid is left maximally compressed with no gravitational potential to fight as it turns around (see Fig. 6) [6]. The net effect is doubled by the metric stretching effect from Φ , leading to fluctuations with amplitude $2\Psi(0) - [\Theta + \Psi](0) = \frac{3}{2}\Psi(0)$.

When the universe becomes matter-dominated the gravitational potential no longer reflects photon density perturbations. As discussed in §5, $\Theta + \Psi = \Psi/3 = 3\Psi(0)/10$ here, so that across the horizon scale at matter radiation equality the acoustic amplitude increases by a factor of 5.

This effect mainly measures the matter-to-radiation ratio. Density perturbations in any form of radiation will stop growing around horizon crossing and lead to this effect. For the neutrinos, the only difference is that anisotropic stress from their quadrupole anisotropies also slightly affects the cessation

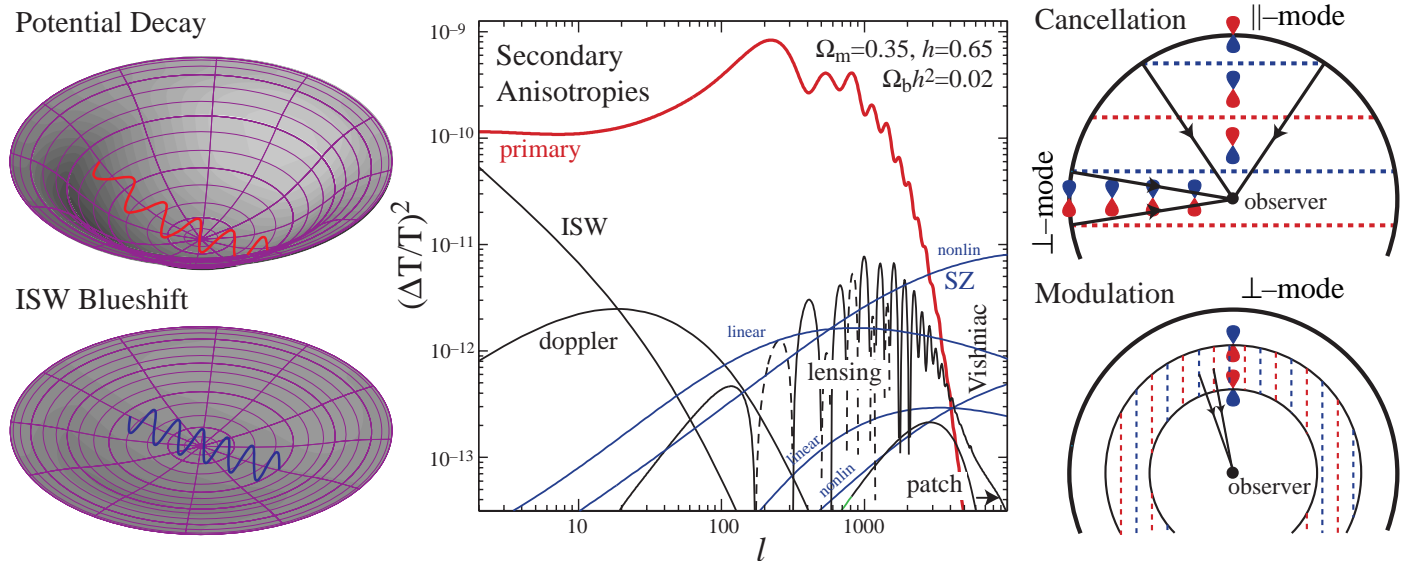


Fig. 7: Secondary anisotropies.

of growth. One can only turn this into a measure of $\Omega_m h^2$ by assuming that the radiation density is known through the CMB temperature and the number of neutrino species otherwise we are faced with a *matter-radiation* degeneracy. For example, determining both $\Omega_m h^2$ and the number of neutrino species from the CMB alone will be difficult.

Precise measurements of $\Omega_m h^2$ when combined with the angular diameter distance would constrain the universe to live on a line in the classical cosmological parameter space $(\Omega_m, \Omega_\Lambda, h)$. *Any* external (non-degenerate) measurement in this space $(\Omega_m, h, \text{acceleration}, \dots)$ and allows the three parameters to be determined independently. This fortunate situation has been dubbed “cosmic complementarity” and currently shows “cosmic concordance” around a Λ CDM model. More importantly, the combination of several checks creates sharp consistency checks that may even show our universe to live outside this space, for example if the missing energy is not Λ but some dynamical “quintessence” field.

9 And Beyond

The primary anisotropies from the recombination epoch contain only a small fraction of the cosmological information latent in the CMB. Let us conclude this survey with topics of future study: secondary anisotropies and polarization. Both are expected to be at the $\lesssim 10^{-6}$ (μK) level and will require high sensitivity experiments with wide-frequency coverage to reject galactic and extragalactic foregrounds of comparable amplitude.

Secondary Anisotropies: These are generated as photons travel through the large-scale structure between us and recombination. They arise from two sources: gravity and scattering during reionization. It is currently believed that the universe reionized at $5 \leq z \lesssim 15$ leading to $\tau_{\text{rei}} \sim 0.01 - 0.1$.

Gravitational redshifts can change the temperature along the line of sight. Density perturbations cease to grow once either the cosmological constant or curvature dominates the expansion. As discussed in §8, the gravitational potentials must then decay. Decay of potential well both removes the gravitational redshift and heats the photons by “metric stretching” leading to an effect that is $2\Delta\Phi$ (see Fig. 7). The opposite effect occurs in voids so that on small scales the anisotropies are cancelled

across crests and troughs of modes parallel to the line-of-sight. The effect from the decay is called the ISW effect [8] and from the non-linear growth of perturbations, the Rees-Sciama [17] effect.

The gravitational potentials also lens the CMB photons [18]. Since lensing conserves surface brightness, it only affects anisotropies and hence is second order. The photons are deflected according to the angular gradient of the potential integrated along the line of sight. Again the cancellation of parallel modes implies that large-scale potentials are mainly responsible for lensing and cause a long-wavelength modulation of the sub-degree scale anisotropies. The modulation is a power preserving smoothing of the power spectrum which reduces the acoustic peaks to fill in the troughs. Not until the primary anisotropies disappear beneath the damping scale do the cancelled potentials actually generate power in the CMB.

The same principles apply for scattering effects – with one twist. The Doppler effect from large-scale potential flows, which run parallel to the wavevector, contribute nothing to the cancellation-surviving perpendicular modes (see Fig. 7). Thus even though $v_b\tau \sim 10^{-4} - 10^{-5}$, Doppler contributions are at 10^{-6} . The main effect of reionization is to suppress power in the anisotropies as $e^{-2\tau}$ below the angle subtended by the horizon at the scattering. Unfortunately, given the sample variance of the low- ℓ multipoles [see eqn. (2)], this effect is nearly degenerate with the normalization and the current limits from the first peak that $\tau_{\text{rei}} \lesssim 1$ will not be improved by more than a factor of a few from the higher peaks.

Surviving the Doppler cancellation are higher order effects due to optical depth modulation, perpendicular to the line of sight, of the Doppler shifts at small angular scales from linear density perturbations (Vishniac effect [19]), non-linear structures (non-linear Vishniac effect or kinetic SZ effect [20]) and patchy or inhomogeneous reionization [21]. Another opacity-modulated signal is the distortion from Compton upscattering by hot gas, the (thermal) Sunyaev-Zel’dovich (SZ) effect [22], especially in clusters where it is now routinely detected.

All of these secondary effects produce signals in the μK regime. Developing methods to isolate them is currently an active field of research and lies beyond the scope of this review. The main lines of inquiry are to explore sub-arcminute scales where the primary anisotropies has fallen off, the non-Gaussianity of the higher order effects [23], their frequency dependence to separate them from foregrounds and the thermal SZ effect [24], their cross correlation with other tracers of large-scale structure [25], and finally their polarization.

Polarization: Thomson scattering of quadrupole anisotropies generates linear polarization in the CMB by passing only one component of polarization of the incident radiation (see Fig. 8). The polarization amplitude, pattern, and correlation with the temperature anisotropies themselves is thus encapsulated in the quadrupole anisotropies at the scattering. This information and the fact that it is only generated by scattering are the useful properties of polarization.

Density perturbations generate quadrupole anisotropies as radiation from crests of a temperature perturbation flows into troughs. Such anisotropies are azimuthally symmetric around the wavevector (Y_{20} quadrupole). They generate a distinct pattern where the polarization is aligned or perpendicular to the wavevector (“ E ” pattern [26]).

However polarization generation suffers from a catch-22: the scattering which generates polarization also suppresses its quadrupole source (see §4). They can only be generated once the perturbation becomes optically thin. Primary anisotropies are only substantially polarized in the damping region where the finite duration of last scattering allows viscous imperfections in the fluid, and then only at the $\sim 10\%$ level (μK level, Fig. 8). Nonetheless its steep rise toward this maximum is itself interesting

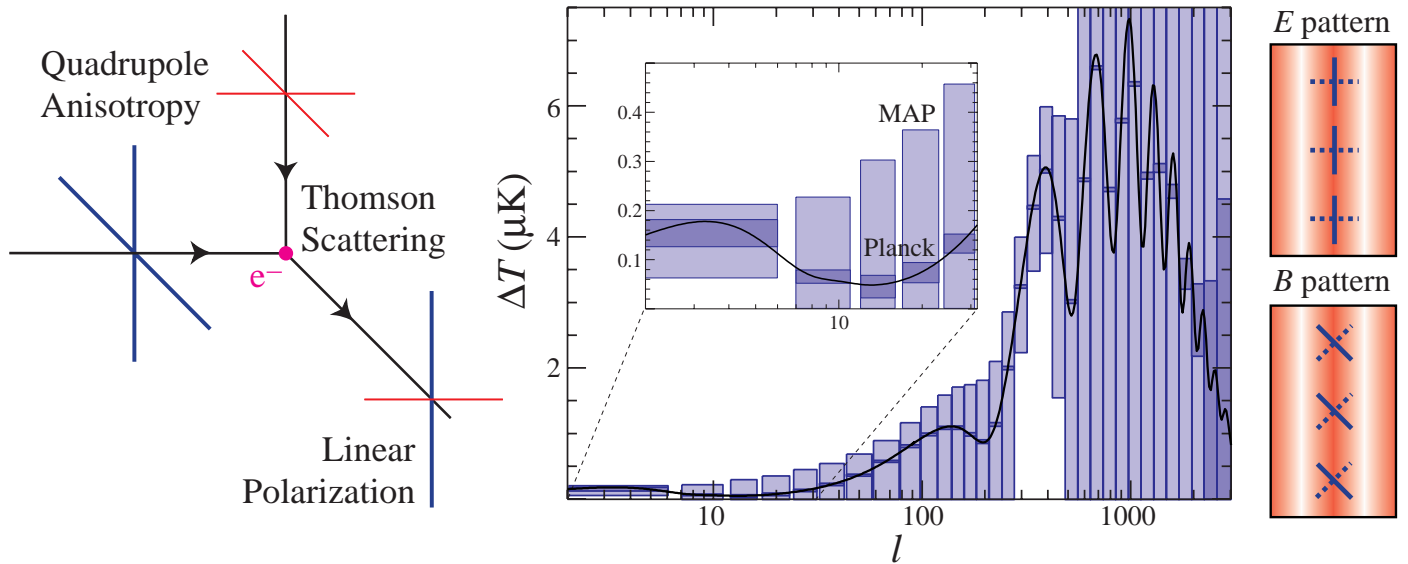


Fig. 8: Polarization.

[28, 27]. Since polarization isolates the epoch of scattering, we can directly look above the horizon scale and test the causal nature of the perturbations (see §5). Likewise, polarization at even larger scales can be used to measure the epoch and optical depth during reionization [29] but will require the sub μK sensitivities of Planck and future missions.

Finally the “ E ” pattern of polarization discussed above is a special property of density perturbations in the linear regime. Its complement (“ B ” pattern) has the polarization aligned at 45° to the wavevector. Vector (vorticity) and tensor (gravity wave) perturbations generate B -polarization as can be seen through the quadrupole moments they generate ($Y_{2\pm 1}$ and $Y_{2\pm 2}$ respectively [28, 30]). Measuring the properties of the gravity waves from inflation through the polarization is our best hope of testing the particle physics aspects of inflation (see e.g. [31]).

B -polarization is also generated by non-linear effects where mode coupling alters the relation between the polarization direction and amplitude. In the context of the simplest inflationary models, the largest of these is the gravitational lensing of the primary polarization [18] but opacity-modulated secondary Doppler effects also generate B -polarization [20].

10 Discussion

We are already well on our way to extracting the cosmological information contained in the primary temperature anisotropies, specifically the angular diameter distance to recombination, the baryon density, the matter-radiation ratio at recombination, and the “acausal” (inflationary) nature and spectrum of the initial perturbations. Even if our simplest inflationary cold dark matter model is not correct in detail, these quantities will be measured in the next few years by long-duration ballooning, interferometry and the MAP satellite, *if the acoustic nature of the peak at $\ell \sim 200$ is confirmed by the detection of a second peak*. In the long term, the high sensitivity and wide frequency coverage of the Planck satellite and other future experiments should allow CMB polarization and secondary anisotropies to open new windows on the early universe and large-scale structure.

Acknowledgements: I would like to thank my collaborators through the years, especially N. Sugiyama and M.

White, the organizers of RESCEU 1999, and the Yukawa Institute for its hospitality. This work was partially supported by NSF-9513835, the Keck Foundation, and a Sloan Fellowship.

References

1. Smoot G. et al. 1992, ApJL 396, L1
2. Scott D., Silk J., White M. 1995, Science 829
3. Tegmark M., Zaldarriaga M. astro-ph/0002091; Knox L., Page L astro-ph/0002162; Melchiorri A., et al., astro-ph/9911445; Miller A.D. et al. 1999, ApJ 524, 1
4. Jungman G., Kamionkowski M., Kosowsky A., Spergel D.N. 1996, PRD, 54, 1332; Bond J.R., Efstathiou G., Tegmark M. 1997, MNRAS 291, L33; Zaldarriaga M., Spergel D.N., Seljak U. 1997, ApJ 488, 1; Eisenstein D.J., Hu W., Tegmark M. 1999, ApJ 518, 2
5. Peebles P.J.E., Yu J.T. 1970, ApJ 162, 815; Doroshkevich A.G., Zel'dovich Ya.B., Sunyaev R.A. 1978, Sov. Astron. 22, 523; Bond J.R., Efstathiou G. 1984, ApJ 285, L45
6. Hu W., Sugiyama N. 1995, ApJ 444, 489; Hu W., White M. 1996, ApJ 471, 30; Hu W., Sugiyama N., Silk J. 1997, Nature 386, 37
7. Seljak U. 1994, ApJ 435, 87
8. Sachs R.K., Wolfe A.M. 1967, ApJ 147, 73
9. Albrecht A., Coulson D., Ferreira P., Magueijo J., PRL 76, 1413.
10. Hu W., White M. 1996, PRL 77, 1687;
11. Turok N.G. 1996, PRL 77, 4138; Hu W., Spergel D.N., White M. 1997, PRD 55, 3288
12. Hu W 1999, PRD 59 021301; Hu W., Peebles, P.J.E. 2000, ApJ 528, 61
13. Hu W., Sugiyama N.1995, PRD 51, 2599
14. Hu W., White M. 1997, ApJ 479, 568
15. Kamionkowski M., Spergel D.N., Sugiyama N. 1994, ApJ 434, L1
16. Silk J. 1968, ApJ 151, 459
17. Rees M.J., Sciama D.N. 1968, Nature, 217, 511; Seljak U. 1996, ApJ, 460, 549
18. Seljak U. 1996, ApJ 463, 1; Zaldarriaga M., Seljak U., 1998, PRD 58, 023003 (1998); Hu W. 2000, astro-ph/0001303
19. Vishniac E.T. 1987, ApJ, 322, 597; Hu W., White M. 1996, A&A, 315, 33
20. Hu W. 2000, ApJ, 529, 12
21. Aghanim N., Desert F.X., Puget J.L., Gispert R. 1996, A&A, 311, 1; Gruzinov A., Hu W. 1998, ApJ, 508, 435; Knox L., Scoccimarro R., Dodelson S. 1998, PRL, 81, 2004; Bruscoli M., Ferrara A., Fabbri R., Ciardi B, astro-ph/9911467
22. Sunyaev R.A., Zel'dovich Ya. B. 1980, MNRAS, 190, 413
23. Goldberg D.M., Spergel D. N. 1999, PRD, 59, 103002; Zaldarriaga M., Seljak U. 1999, PRD 59, 123507; Cooray A.R., Hu W. 1999, ApJ in press, astro-ph/9910397
24. Bouchet F., Gispert R., 1999, NewA, 4 443; Tegmark M., Eisenstein D.J., Hu W., de Oliveira-Costa A. ApJ, 1999, in press, astro-ph/9905257; Cooray A., Hu W., Tegmark M. astro-ph/0002238
25. Sugihara M., Sugihara T., Spergel D.N., 1998, ApJ 495 511; Waerbeke L.V., Bernardeau F., Benabed K. 1999, astro-ph/9910366; Peiris H.V., Spergel D.N., astro-ph/0001393
26. Kamionkowski M., Kosowsky A., Stebbins A. 1997, PRD 55, 7368; Zaldarriaga M., Seljak U. 1997, PRD 55, 1830
27. Spergel D.N., Zaldarriaga M. 1997, PRL 79, 2180
28. Hu W., White M. 1997, PRD 56, 596
29. Hogan C.J., Kaiser N., Rees M.J. 1982, Phil. Trans. R. Soc. Lond. A307, 97
30. Hu W., White M. 1997, NewA 2 323
31. Kamionkowski M., Kosowsky A. astro-ph/9904108

This figure "baryon.gif" is available in "gif" format from:

<http://arxiv.org/ps/astro-ph/0002520v1>

This figure "curv.gif" is available in "gif" format from:

<http://arxiv.org/ps/astro-ph/0002520v1>

This figure "matter.gif" is available in "gif" format from:

<http://arxiv.org/ps/astro-ph/0002520v1>

This figure "tau.gif" is available in "gif" format from:

<http://arxiv.org/ps/astro-ph/0002520v1>